TWENTY FIRST EUROPEAN ROTORCRAFT FORUM

PAPER No. 2-3

PRELIMINARY RESULTS FROM A THREE-DIMENSIONAL DYNAMIC STALL EXPERIMENT OF A FINITE WING

R.A.McD. GALBRAITH, F.N.COTON, D. JIANG & R. GILMOUR
Department of Aerospace Engineering,
University of Glasgow, Scotland, U.K.

August 30 - September 1, 1995
SAINT-PETERSBURG, RUSSIA

Paper nr.: II.3

Preliminary Results from a Three-Dimensional Dynamic Stall Experiment of a Finite Wing.

R.A. McD. Galbraith; F.N. Coton; D. Jiang; R. Gilmour

TWENTY FIRST EUROPEAN ROTORCRAFT FORUM
August 30 - September 1, 1995 Saint-Petersburg, Russia

SUMMARY

This paper describes an experiment to assess the surface pressure distribution on a finite wing whilst undergoing rapid pitch motions.

Apart from describing the test facility, typical data from a high speed ramp-up motion to beyond stall is discussed. The data clearly illustrate the three-dimensionality of the flow, including the tip vortex, when compared to its nominally two-dimensional counterpart. Although only ramp-up data are presented in this paper, other tests performed included oscillatory and ramp-down motions.

INTRODUCTION

Almost all the early dynamic-stall tests have been performed under nominally two-dimensional flow conditions. One of the early works by Moss and Murdin [1](1968) clearly showed that, although the flow was nominally two-dimensional for the fully attached steady flow case, the stall cells were highly three-dimensional. The perceived need to have a better insight into the phenomena associated with dynamic stall encouraged many more experimenters to design and develop their own research facilities. Of particular note are the works of McCroskey et al [2], McAllister et al[3], Petot[4], Wood[5], Carta et al[6] and the associated attempts to reconstruct or model the measured data; in Britain the modelling has been predominated by Westland Helicopters and, in particular, the Beddoes[7] methodologies. From these works and several others, Young[8] proposed a good description of the characteristic phenomena associated with dynamic stall.

Although Young's description has been generally accepted as a fair assessment, the totality of the process is still poorly understood. For example, two seemingly equivalent experiments[9, 10] have yielded contradictory results pertaining to the effect of pitch rate on the convection velocity of the dynamic stall vortex. Green and Galbraith[11], who spent much effort assessing both the data sets involved, concluded that, if the geometric environment of the experiments was similar, the difference was most likely associated with the respective Mach numbers; 0.17[10] and 0.3[9].

It had also been noted that, during ramp-down motions, the re-establishment of fully attached flow was delayed and could result in negative values of lift at large incidence, [Refs. 12,13].

Albeit there were anomalies to be reconciled and a better understanding of the effect of Mach number, Reynolds number and tunnel environment required, the data have been put to good use in the development of dynamic stall models[14,15,16,17]. Those models are predominantly two-dimensional and, although they can be modified to cope with the three-dimensional planform in the region of the tip[18], there are very little data and detailed understanding with which to test and develop those preliminary attempts.

The region of the tip is further complicated by the new planforms including the so-called BERP tip. These tips can have highly swept leading edges and so there arises a fundamental difference between the stalling pattern at the tip and

over the larger part of the rotor. The swept tip may be dominated, on the retreating side of the rotor disc, by a strong vortex similar to that of a delta wing whilst the inner portions, may possess a flow typical of the two-dimensional test case. The manner in which the straight wing and the delta wing stall dynamically is fundamentally different and the basic questions to be addressed are, what are the differences between the dynamic stalling of a finite straight wing and that of a delta wing together with manner in which both associated phenomena interact for a straight wing with highly swept tips.

Data pertaining to the above questions require the execution of three-dimensional dynamic stall experiments of which, to date, there are but a few.
Some foresighted flow visualisation experiments were carried out at C.U. Boulder[19] investigating both the manner of the stall and the associated connectivity of vortical structures. A more involved experiment was carried out by Pezali[20] at NASA Ames and involved a cantilevered finite wing heavily instrumented with pressure transducers. For the past three years the authors have been developing a three-dimensional dynamic-stall facility in which the first three finite wings to be tested will have a straight planform, a delta wing and a straight wing with swept tips at an angle equal to that of the delta wing.

This paper presents a description of the facility developed at Glasgow and the results from a single test case from the straight wing. Those results are for a rapid ramp-up motion and the data were collected from over 200 channels of which 193 were pressure transducers.

The flow considered exhibits the hallmark of nominally two-dimensional pressure histories close to the mid-span and quite different pressure profiles as the tip is approached. There appears to be a fascinating complexity of vortex/vorticity connectivity that may be confirmed with good flow visualisation along the same lines as the work carried out at Boulder.

It is anticipated that the data collected will have three prime uses.

1. Assist in the understanding and description of the associated flow phenomena.
2. Allow further development of semi-empirical models for dynamic stall.
3. For the validation or otherwise of "CFD" codes.

DESCRIPTION OF THE GLASGOW FACILITY

The facility developed is housed in the 2.13 x 1.61 metre octagonal working section of the Department's low-speed closed-returned wind tunnel. Figure 1 is a schematic of the general set-up where it may be seen that the wing is mounted centrally in the working section and actuated by two supports to the rear. The main support structure is beneath the tunnel and contains both an actuation mechanism and the angular displacement transducer.

The model's aerofoil section was that of a NACA 0015 and the tips were simple solids of revolution. The overall dimensions were 126 cm x 42cm giving an overall aspect ratio of 3. The model was constructed with an aluminium framework of ribs and stringers with an outer epoxy glass fibre skin. Figure 2 illustrates this construction

and the associated transducer placements.

Overall 192 pressure transducers were placed within the model predominantly to the starboard side. There were six chordal distributions at various spanwise location, each of which had up to 30 transducers. In the region of the tip, additional transducers were placed between the above mentioned sections in order to provide a better assessment of the tip vortex movement and structure. As a check on the overall symmetry of the flow, five transducers were placed on the port side of the wing in corresponding positions to their counterparts on the starboard side. Additionally three accelerometers were embedded in the wing, two of which were at the rear tip locations and a final one mounted centrally.

All transducers were of Kulite differential type CJQH-187 and significant tubing was required to ensure the rear of the diaphragms were maintained at the external atmospheric pressure. The signals from all of these transducers were taken to a specially designed signal conditioning unit of modular construction with each module containing its own control board. On instruction from the computer, the control board automatically removes all offsets to below the A-D converter resolution and on further instruction adjust all gains as necessary. In fact, during a test the computer sampled the maximum and minimum of each transducer output and adjusted the gains accordingly to improve the data acquisition resolution. The computer used contained a 486 processor and interfaced with the proprietary Backer BE256 modular data acquisition system. As configured, the Glasgow system contains 200 channels of analogue to digital conversion, each of which is capable of sampling to a maximum rate of 50 kHz, giving an overall sampling rate of 10MHz.

A large sampling rate was required to capture the fine detail of the dynamic stall process, especially when the reduced pitch rates or reduced frequencies were relatively high. For example, at the reduced frequency of 0.18, where the oscillation frequency at 50 m/sec wind speed is approximately 7Hz, the overall sampling rate was in the region of 30 kHz per channel.

THE TEST SEQUENCE

For the straight finite wing, four particular test motions were considered. The first of these was to assess the steady performance of the aerofoil over the entire incidence range of -5^{o} to $+40^{o}$. This was carried out at regular intervals as a check on the overall system performance. Second, a ramp-up sequence in which the aerofoil was pitched up at a constant rate. For the lower pitch rates, excellent ramp functions are obtained but, as can be imagined, at the higher values the starting and stopping sequences induce non-linearities. Nonetheless, over the area of interest, i.e., stall initiation, the pitch rates remain relatively constant. Third, a ramp-down in which the aerofoil is exposed to a constant negative pitch rate and, finally, a series of oscillatory tests more typical of extant dynamic stall experiments. In all approximately 100 test cases were considered, albeit the total runs exceeded this number.

RESULTS

The full test matrix for the rectangular wing planform is

presented in Table 1. In this section, data from a single test case will be presented in the form of pressure distributions and integrated force and moment coefficient variations. The particular case is that of a ramp-up between -5 and +38 degrees at a linear pitch rate of 411 degrees per second. Whilst being a particularly interesting case, it also serves to illustrate the quality of the data and the range of information available from the study. It should be noted that of the 8000 measurements taken at each transducer location during an individual test, only one in forty or one in eighty of the points are plotted on the graphs presented. Use of higher resolution, whilst beneficial when examining a specific feature of short-duration, is limited by line thickness when surface plotting over the entire incidence range.

As indicated above, most of the 192 pressure transducers were located on the right hand side of the wing. A small number were, however, positioned on the left semi-span to give an indication of the symmetry of the wing loading. In Fig. 3. the pressure signals at two locations on the left hand side of the wing are compared with the corresponding measurements from the main transducer array. The transducers located at 90% of span were near the leading edge and, as may be expected, showed good agreement up to the bluff-body state. Conversely, at 65% of span, the symmetry check was conducted at approximately 50% of chord. Once again, the symmetry is exceptional up to around 30 degrees. Beyond this, there is a substantial surge in the measured suction followed by a rapid pressure recovery. Throughout these changes, however, there is still a high degree of symmetry apparent in the pressure traces.

Figure 4 presents the variations of the local normal force coefficients at the six instrumented span locations. In each case, the measured static characteristic at the particular spanwise station is provided for reference. A feature common to all of the plots is the incidence reversal after the end of the ramp motion. This was caused by limitations of the hydraulic system and was a control response to an initial overshoot at the end of the ramp phase. Previous studies have shown, however, that the dominant features of the unsteady flowfield appear relatively insensitive to this type of behaviour[11]. Nevertheless, it is pertinent to note that only the very fast ramp cases, where the hydraulic actuation system was operating at its design limit, were affected in this way.

At the 57.14% span location, the normal force produced during the ramp motion follows the general trend of, but marginally exceeds, its static counterpart up to the static stall incidence. Beyond this, there is the classical dynamic overshoot as the Cn build up continues in a monotonic manner until approximately 26 degrees where there is a marked increase in the gradient of the curve. This increased rate of Cn growth is short lived and is followed by a fairly benign stall at around 33 degrees.

The trends exhibited at the 68.1% span location are broadly similar to those identified above. In this case, however, the marked increase in the Cn gradient after 26 degrees is sustained for a much longer period and stall is delayed to 39 degrees. As a consequence, the peak Cn is much higher and the

stall is very sharp. This behaviour is largely reproduced at 80% of span except that the peak Cn is sustained for a longer period.

As may be observed from the data presented for 90% and 94.6% of span, the Cn gradient at low incidence becomes progressively lower and the linear portion of the curve is reduced in line with the trends in the static data as the wing tip is approached. Additionally, the pre-stall increase in gradient witnessed in the previous cases becomes less pronounced. The combination of these features produces a reduction in the peak Cn on these outboard sections. This trend continues to the final measurement station at 97.2% of span where the non-linearity at low incidence is particularly evident. It is also significant that the Cn curve corresponding to this location has a much higher noise content than those of the inboard sections.

In Fig. 5. the spanwise distributions of local Cn, Ct and Cm are plotted against the temporal change in incidence. To aid analysis, the data obtained on the fully instrumented side of the wing is reflected to give a full spanwise loading distribution. This allows features of the graph which may be hidden by the viewing angle to be more clearly identified on the other half of the span.

The variation of the spanwise Cn distribution is consistent with the observations made above. In particular, the earlier stall at the mid-span is clearly evident as is the delayed stall at higher Cn between 60% and 80% of span. This behaviour is generally reproduced in the Ct graph although differences are apparent in the tip region. In particular, the build-up of Ct at the 97.2% of span location is minimal across the incidence range.

The graph of the pitching moment coefficient, Cm, displays most of the salient features of the other two plots. At inboard sections, the build up in Cn prior to stall is associated with a sharp downward 'break' in Cm. Towards the tip, however, this 'break' is less pronounced and the negative progression of Cm is more uniform.

The force and moment coefficients presented above were obtained by integration of chordwise pressure distributions at the relevant spanwise locations. It has been shown[12,13], for ramp-down motions, that the most significant features of these pressure distributions are manifest on the upper surface. Figure 6 illustrates the variation of the upper-surface chordwise pressure distribution, with the temporal change in incidence, at three of the spanwise positions, discussed above.

At 57.14% of span, the pressure distribution is characterised by the classical growth of leading edge suction as the incidence increases. Additionally, there is no obvious sign of trailing edge separation, even above 20 degrees. At approximately 30 degrees the leading edge suction peak begins to collapse. At the same time, a suction bulge develops just behind the leading edge and then moves rearwards with time. During its progression towards the trailing edge, this suction bulge loses definition but can be clearly observed leaving the trailing edge after the end of the ramp. After this, a second area of suction appears near the quarter chord and moves towards the trailing edge, losing definition as it goes.

At the 80% span location, the initial behaviour of the chordwise pressure distribution is similar to that at 57.14%. In particular, the leading edge suction peak grows with increasing incidence and, once again, trailing edge separation is suppressed. In this case, however, the suction peak attains a slightly higher value than the previous case and its subsequent collapse is less rapid. At approximately 36 degrees there is evidence of a small area of increased suction developing near the 15% chord location. At this point, this localised suction is poorly defined but, unlike the previous case, it increases in size and strength as it moves rearwards. By the time the disturbance reaches the 50% chord location it is considerably stronger than its counterpart at 57.14% span. Its strength continues to increase before diminishing slightly as it passes over the trailing edge. Unlike the previous case, there is no clear evidence of a secondary area of suction.

The final plot in Fig. 6. shows the behaviour of the pressure distribution at the 97.2% of span position near the wing tip. In this case, the build up of suction at the leading edge is much less significant than the previous two cases. It is, however, accompanied by a build up of suction at the trailing edge which starts at very low positive incidence. As the ramp progresses; this area of suction increases in strength and occupies more of the chord until finally it disappears as the suction peak collapses. Subsequently, there is a slight recovery of suction at the leading edge before a secondary collapse.
An alternative view of these processes may be obtained by study of the temporal variation of the spanwise pressure distributions at specific chordwise locations. Figure 7 presents this information at 17%, 37% and 83% of chord. Here the data from the fully instrumented semi-span has been reflected to give a full spanwise distribution of pressure.

The development of the areas of localised suction discussed above are clearly evident at the 17% chord location. In this case, the first indications occur near the mid span and are followed by disturbances of longer duration between 60% and 80% of span. Further outboard, however, any apparent increased suction is on a much smaller scale and is indistinct.

At 37% of chord, the localised areas of suction are again apparent and exhibit the same trends as the previous chordal position. In this case, however, the secondary suction bulge identified at 57.14% of span can be observed. Unlike the initial disturbance, this secondary area of suction is most significant near the centre span. Another feature of note at this chordal position is the steady increase in suction at the wing tips. This corresponds to the area of suction which develops at the trailing edge near the wing tip and spreads forward with increasing incidence. It is even more apparent in the final graph of Fig. 7. for the 83% chord position where it can be observed to affect a larger portion of the span. At 83% of chord, however, the convecting suction bulge is poorly defined near the centre span but is substantially enhanced at around 80% of the span. This is consistent with the features identified at in Fig. 6.

DISCUSSION

The flow behaviour and loading distributions associated with a pitching wing are complex and cannot fully be interpreted on the basis of pressure data alone. The present study can, however, provide valuable insight into the basic mechanisms which interact to produce the features identified in the previous section. Since most of the earlier studies on dynamic stall have concentrated on the nominally two-dimensional case, there is little detailed information available on three-dimensional effects. Nevertheless, it may be anticipated that the basic features of the nominally two-dimensional case will be present, in some form, towards the mid-span of the wing and that the tip region will be subject to the influence of the wing tip vortex. The nature of the connectivity between these two regions remains to be addressed.

In steady flow, the spanwise loading distribution on a finite wing is dominated by the downwash from the wing tip vortices which becomes more significant nearer the wing tips and acts to reduce the effective incidence there. This is clearly illustrated in Fig.4. where the gradient of the steady flow Cn curves is lower on outboard sections than those close to the mid span. If this effect was reproduced during ramp-up motion, an inevitable consequence would be a spanwise variation of effective pitch rate on the wing. Evidence of this can be observed in Fig.4. where the Cn curves for the ramp-up case closely follow those measured for steady flow. Given that the ramp motion is nominally linear, this result indicates higher effective pitch rates at the mid span than near the wing tips.

For the nominally two-dimensional case, it is generally accepted that the severity of the dynamic stall process is closely related to pitch rate, with high pitch rates producing the most severe dynamic loadings. It has also been established that a suitable parameter which can be used to relate tests conducted at different wind speeds and pitch rates is the non-dimensional reduced pitch rate, given by $\dot{\alpha}c/2V$. Figure 8 presents the measured Cn curve from a ramp test, on a nominally two-dimensional NACA 0015 aerofoil section, at the same geometric reduced pitch rate as the current test. Despite the spanwise variation in effective reduced pitch rate highlighted above, it may be observed that the main characteristics of this Cn distribution are broadly similar to those presented in Fig. 4 for inboard locations on the three-dimensional model. These common features can, therefore, be explained by reference to contemporary understanding of nominally two-dimensional flows.

In the two-dimensional case, the suppression of trailing edge separation leads to a significant extension of Cn growth beyond the point of static stall. At the reduced pitch rate considered, a strong vortex forms near the quarter chord location and grows in strength before travelling rearwards over the aerofoil. The development of this vortex produces a localised area of increased suction on the upper surface of the aerofoil which, in turn, produces a more rapid increase in Cn. As the vortex begins to move, the leading edge suction peak collapses and Cn stall occurs. Finally, the vortex convects off the trailing edge and flow resembles the bluff body state. The behaviour of this vortex, termed the dynamic stall vortex, is

clearly evident in Fig. 9. where the evolution of the upper surface pressure distribution is presented for the NACA 0015 aerofoil. In the figure, the dynamic stall vortex is manifest as a suction bulge which first appears at approximately 30 degrees incidence. The build-up and subsequent convection of the vortex is easily identified.

As indicated above, many of the basic features of the Cn curves measured in the present study are similar to those of the two-dimensional case. At the 57.14% of span location, it is noticeable that the increased growth in Cn, caused by the dynamic stall vortex, is short lived. This is consistent with the corresponding upper surface pressure distribution variation shown in Fig. 6. where, although the suction bulge of the vortex appears near the leading edge, it is not as great as in the two-dimensional case. There is also very little evidence of vortex build-up with convection occurring almost immediately. At this point, the leading edge suction peak collapses and Cn stall occurs. With the subsequent movement of the dynamic stall vortex, it becomes less distinct and less influential on the post stall Cn. One possible explanation for this behaviour is forthcoming from the work of Horner et al.[19] who conducted flow visualisation experiments on an oscillating flat plate. Their work noted that a dynamic stall vortex did indeed form along most of the span but that the portion of the vortex at the mid-span lifted off the surface during its downstream convection. If this behaviour were repeated in the present case, the influence of the dynamic stall vortex on the measured pressure distribution would be expected to diminish as it lifted away from the surface. Initial convection of the vortex may also be initiated earlier as the vortex becomes more exposed to the influence of the freestream.

The same flow visualisation study also indicated that the segments of the dynamic stall vortex near the 80% of span position initially lifted from the surface before being pushed downwards as the vortex convected. This is, again, consistent with both the relevant Cn curve and the features of the corresponding upper surface pressure distributions shown in Fig. 6. In Fig. 6, the suction bulge, indicative of the dynamic stall vortex, is initially indistinct but becomes more significant as it moves rearwards. At the same time, the collapse of the leading edge suction peak is delayed well beyond that of the two-dimensional case. The resulting effect on the Cn curve is that the change of gradient associated with the formation of the dynamic stall vortex and the magnitude of the peak Cn are less than the two-dimensional case but stall occurs much later.

At most of the span locations presented in Fig. 4, the Cn values measured during the early stages of the ramp motion exceed those obtained in the static test. Conversely, in the two-dimensional case, the dynamic coefficients may be observed to lag the steady values. The precise reason for this inconsistency is unclear but must, inevitably, be a consequence of the spanwise loading distribution on the wing during the pitching motion. From the discussion above, this implies that some aspect of the behaviour of the tip vortices, such as an increase in strength or a lateral inwards movement, may provide the required explanation. More detailed information, such as

flow visualisation or off-body velocity measurements, will be required before any conclusions can be drawn.

A more tangible effect of the tip vortices can be observed in the pressure distribution plot at 97.2% span presented in Fig. 6. Here, and in the results presented for the 83% of chord location in Fig. 7, a substantial increase in suction is witnessed near the wing tips in the vicinity of the trailing edge. This suction is generated by the proximity of the tip vortex and, as the incidence increases, it becomes stronger and influences more of the trailing-edge corner of the wing. Finally, the collapse of leading edge suction and the associated reduction in circulation, rapidly diminishes the tip vortex strength.

One direct consequence of the suction produced by the tip vortex on the aft portion of the chord, is to reduce the build up of Ct. This is evident in Fig. 5. where, although the Cn variation at 97.2% is not much different from the two stations immediately inboard, the corresponding Ct curves are quite different. A similar effect can be observed in the Cm histories where, prior to dynamic stall, the suction produced by the tip vortices results in higher nose down pitching moments on outboard sections.

It is also interesting to note that the Cn curve corresponding to the 97.2% of span position displays a high noise content. Similarly, the Ct and Cm variations near the tip in Fig. 5, exhibit similar behaviour. This appears to be related to pressure fluctuations in the surface region affected by the tip vortex which could be caused by variations in the position of the vortex core or an uneven distribution of discrete vorticity within the developing tip vortex.

CONCLUDING REMARKS

The unsteady surface pressure variations extant on a straight finite wing, undergoing a variety of pitching motions, have been obtained using a new test facility.

Preliminary indications suggest that, although the inboard or mid-span region of the wing behaves in an analogous manner to the nominally two-dimensional counterpart, no such correspondence is observed as the wing tip is approached.

The manner of the overall stall pattern is indeed complex and a full confident prescription of that process requires additional information. In particular the development and subsequent motion of the obvious vortical structures and their associated connectivity. Reference to corresponding flow visualisation has aided the overall interpretation but more detailed studies will be required.

The data appear to be good and it is anticipated that it will have three prime uses.

1. Assist in the understanding and description of associated flow phenomena.
2. Allow further development of semi-empirical models for dynamic stall.
3. For the validation or otherwise of "CFD" codes.

ACKNOWLEDGMENTS

The work was carried out with funding from the Engineering &

Physical Science Research Council, Westland Helicopters, Defence Research Agency and the University of Glasgow. The authors acknowledge with gratitude the help and support of their sponsors.

REFERENCES

[1] Moss,G.F., Murdin,P.W., ' Two Dimensional Low-Speed Tunnel Tests on The NACA 0012 Section Including Measurement Made During Pitch Oscillations at The Stall', RAE Technical Report CP No. 1145, 1968

[2] McCroskey,W.J, and Fisher, R.K. ' Detailed aerodynamic measurements on a model rotor in the blade stall regime', AIAA Journal, Vol. 17, No.1, pp 20-30, 1972.

[3] McAlister, K.W., Carr,L.W.,and McCroskey, W.J. ' Dynamic Stall Experiments on NACA0012 Airfoil', NACA TP-1100, 1978

[4] Petot, J.J., ' Experimental and Theoretical Studies on Helicopter Blade Tips at ONERA', 6th European Rotorcraft and Powered Lift Aircraft Forum, Bristol, 1980

[5] Wood,M.E., ' Results of Oscillatory Pitch and Ramp Tests on the NACA0012 Blade Section', ARA Memo No. 220, December, 1979

[6] Carta,F.O., ' Experimental Investigation of the Unsteady Aerodynamic Characteristics of a NACA 0012 Airfoil', Res. Rep. M-1283-1, United Aircraft Corp., July,1960

[7] Beddoes,T.S., ' A Synthesis of Unsteady Aerodynamic Effects Including Stall Hysteresis', Vertica, Vol. 1, pp 113-123, 1976

[8] Young,W.H.,Jr,' Fluid Mechanics Mechanisms'. NASA -TM- 81956, March 1981

[9] Lorber,R.F., Carta,F.O., 'Unsteady Stall Penetration Experiments at High Reynolds Number', AFOSR TR-87-1202, UTRC R87-956939-3, 1987

[10] Galbraith,R.A.McD, Gracey, M.W. and Leitch, E., 'Summary of Pressure Data for Thirteen Aerofoils on the Database', G.U. Aero Report: 9221, 1992.

[11] Green,R.B,Galbraith,R.A.McD, Niven,A.J.,' Measurements of the Dynamic Stall Vortex Convection Speed', The Aeronautical Journal of The Royal Aeronautical Society, October 1992

[12] Green,R.B,Galbraith,R.A.McD, ' Phenomena Observed during Aerofoil Ramp-Down Motions From The Fully Separated State', The Aeronautical Journal of The Royal Aeronautical Society, November 1994

[13] Green,R.B,Galbraith,R.A.McD, ' Dynamic Recovery to Fully Attached Aerofoil Flow from Deep Stall', Appearing in AIAA Journal

[14] Beddoes,T.S., 'Representation of Airfoil Behaviour', AGARD Specialists Meeting on the Prediction of Aerodynamic Loads on Rotorcraft, AGARD CP-334, 1982, also Vertica, Vol. 7, (2)., 1983

[15] Leishman,J.G., Beddoes,T.S., ' A Semi-Empirical Model for Dynamic Stall', Journal of The American Helicopter Society, July 1989

[16] Gangwani,S.T., ' Synthesised Airfoil Data Method for Prediction of Dynamic Stall and Unsteady Airfoils', Proceedings of the 39th Annual Forum of the America Helicopter Society, 1983, also Vertica, Vol. 8, 1984

[17] Tran,C.T., Petot,D., ' Semi-Empirical Model for The Dynamic Stall of Airfoils in View of The Application to The Calculation of Responses', ONERA T.P. 103-1980.

[18] Beddoes,T.S., ' A 3-D Separation Model For Arbitrary Planforms', 47th Annual Forum of the American Helicopter Society, Phoenix, Arizona, May 1991

[19] Horner,M.B., Addington, G.A., Young III, J.W. and Luttges, M.W., 'Controlled Three-Dimensionality in Unsteady Separation Flows about a Sinusoidally Oscillating Flat Plate', AIAA- 90-0689, Jan. 1990

[20] Piziall, R.A., ' 2-D and 3-D Oscillating Wing Aerodynamics for a Range of Angles of Attack Including Stall', NASA-TM-4632, September 1994

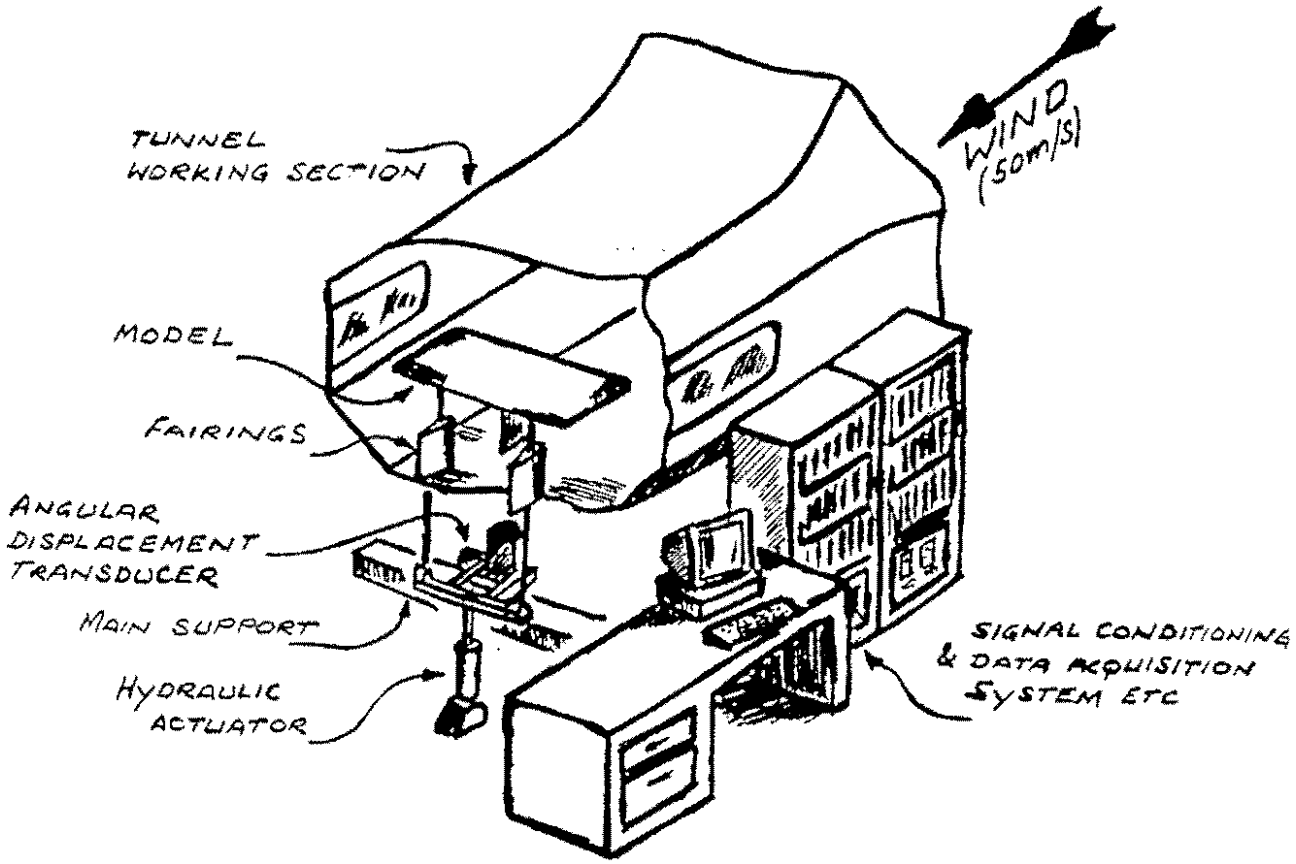

Fig.1 Schematic of Test Set-up

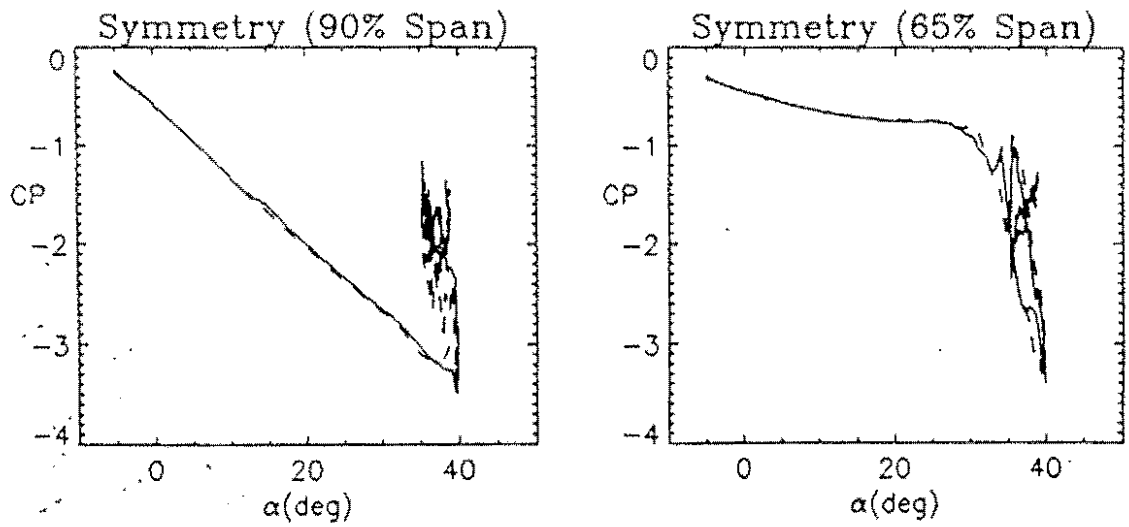

Ramp arc:-5° ~ 38°, Riduced Pitch Rate = 0.0272, Re = 1.475×10^6

Fig.3 Symmetry of Cp Distribution on Upper surface (Ramp up)

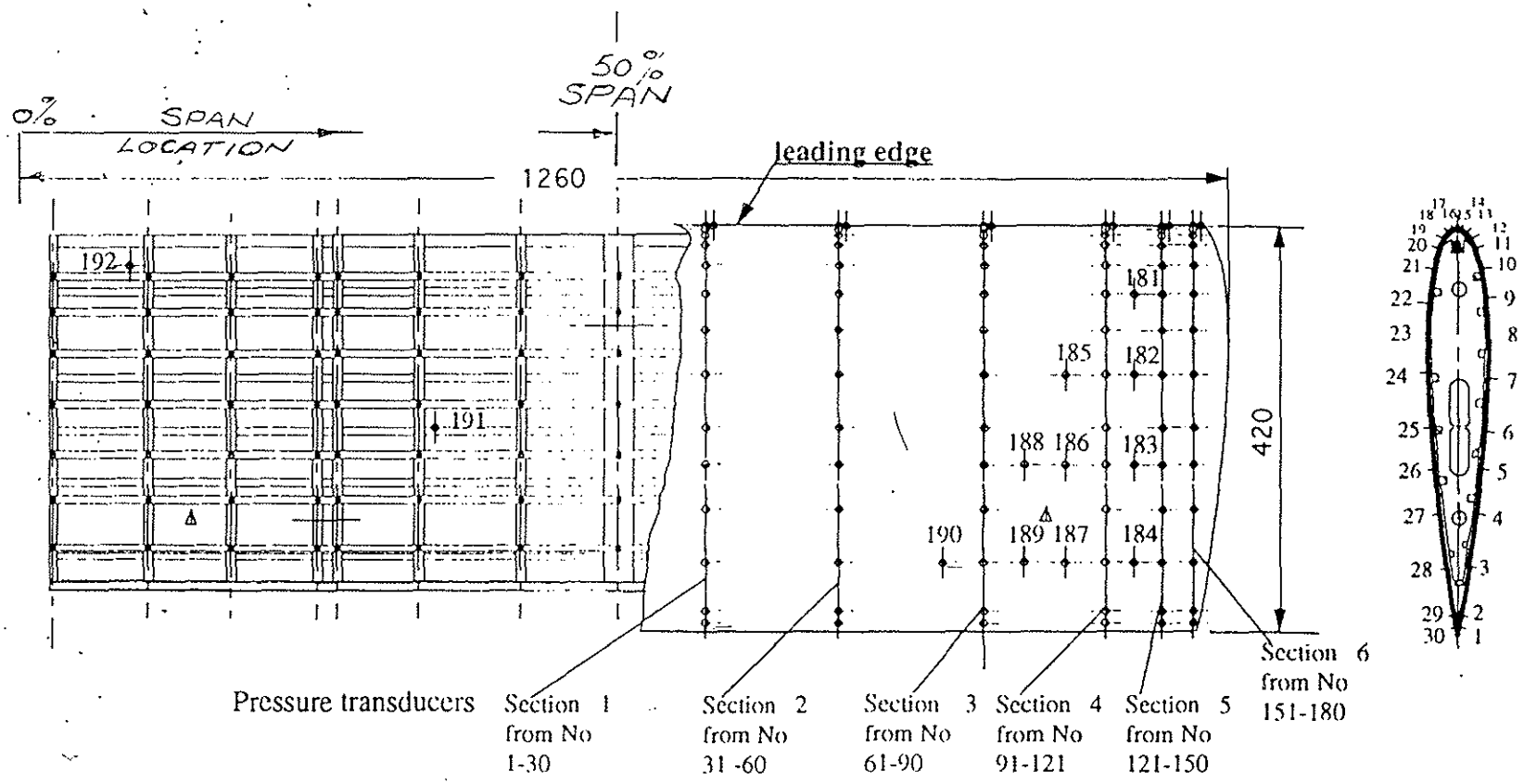

Fig.2 Sketch of Model and Transducers Distribution

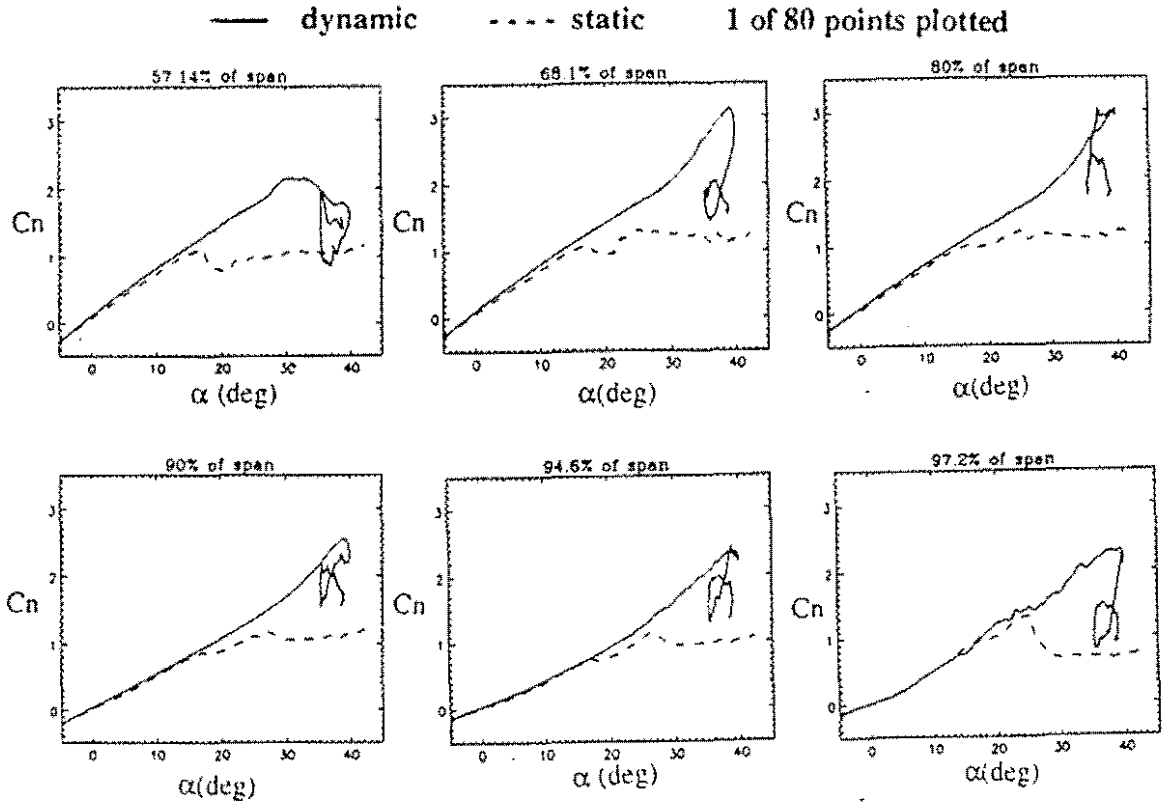

Reduced Pitch Rate = 0.0272, Re = 1.475×10^6

Fig.4 Local Cn against α at different Span Position (Ramp Up)

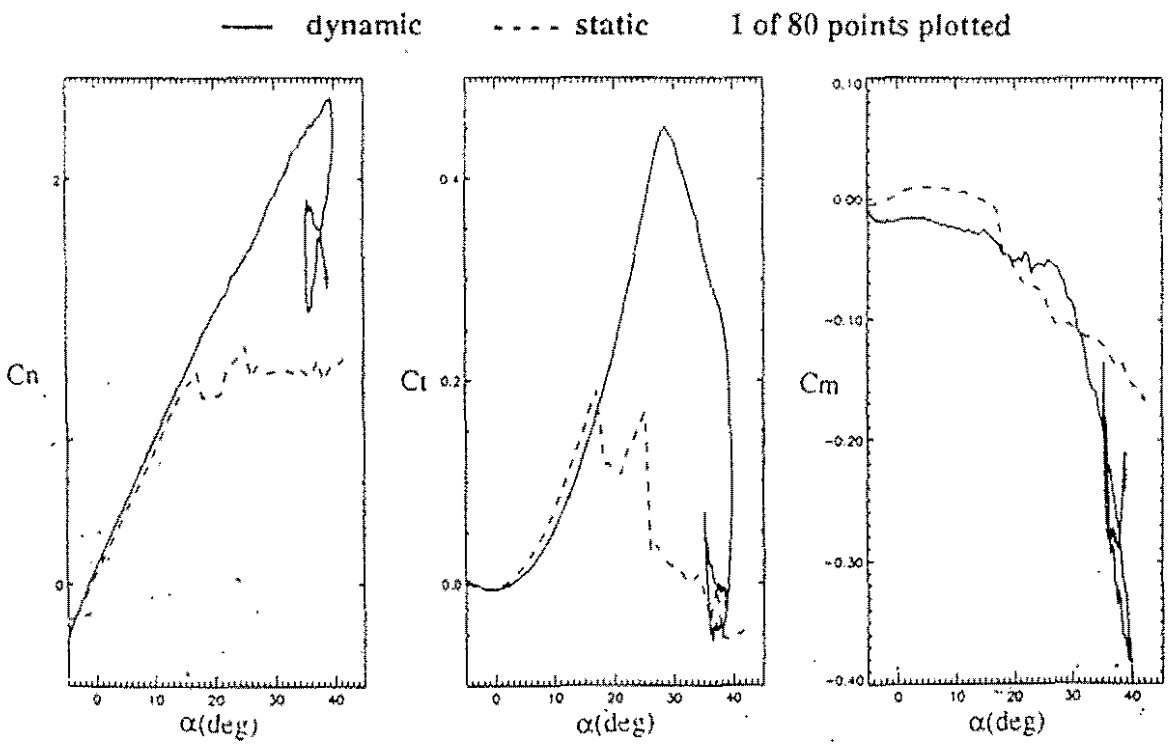

Reduced Pitch Rate = 0.0272, Re = 1.475×10^6

Fig.5 Full Model Cn, Ct, Cm against α (Ramp Up)

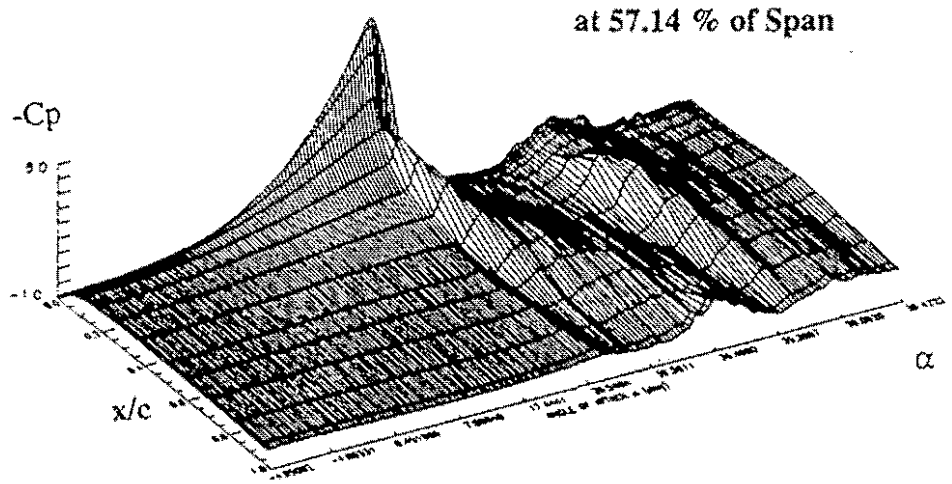

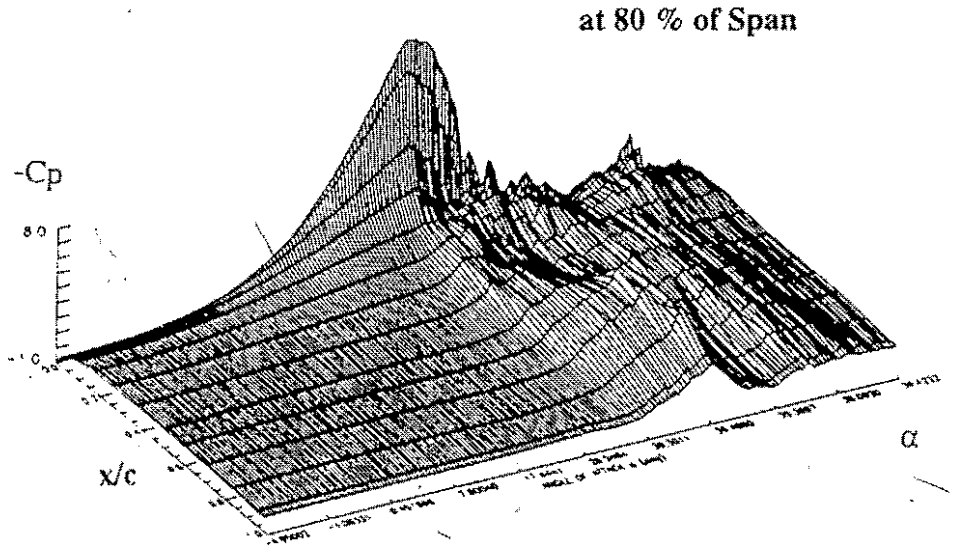

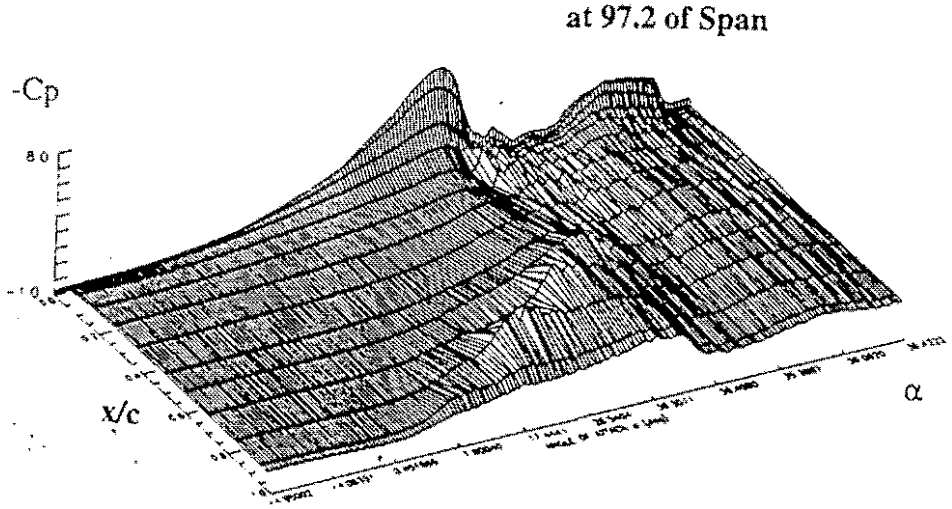

Reduced Pitch Rate = 0.0272, Re = 1.475×10^6

Fig.6 Chordwise Cp Distribution against α (Ramp up)

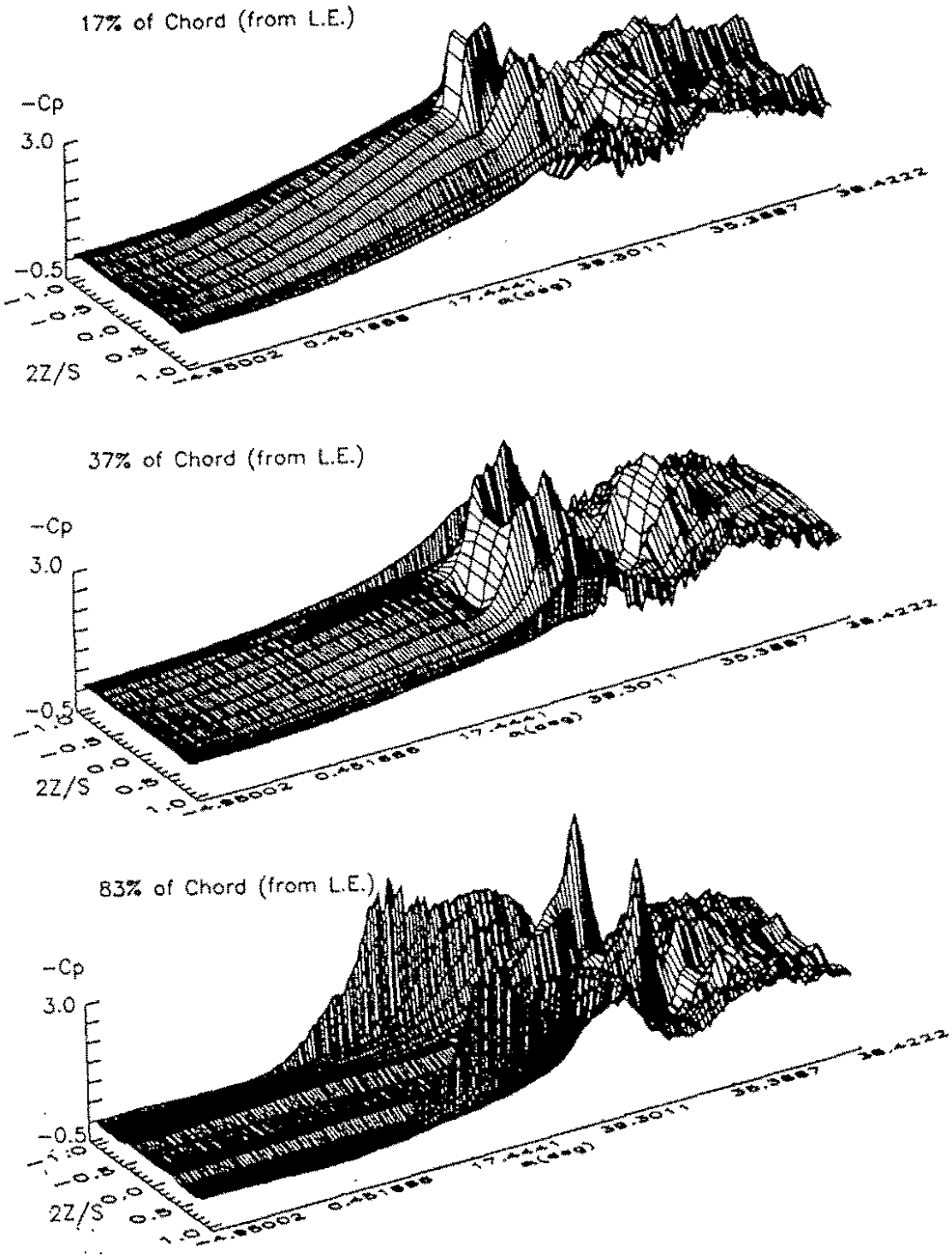

Reduced Pitch Rate = 0.0272, Re = 1.475×10^6

Fig.7 Spanwise Cp Distribution against α (Ramp Up)

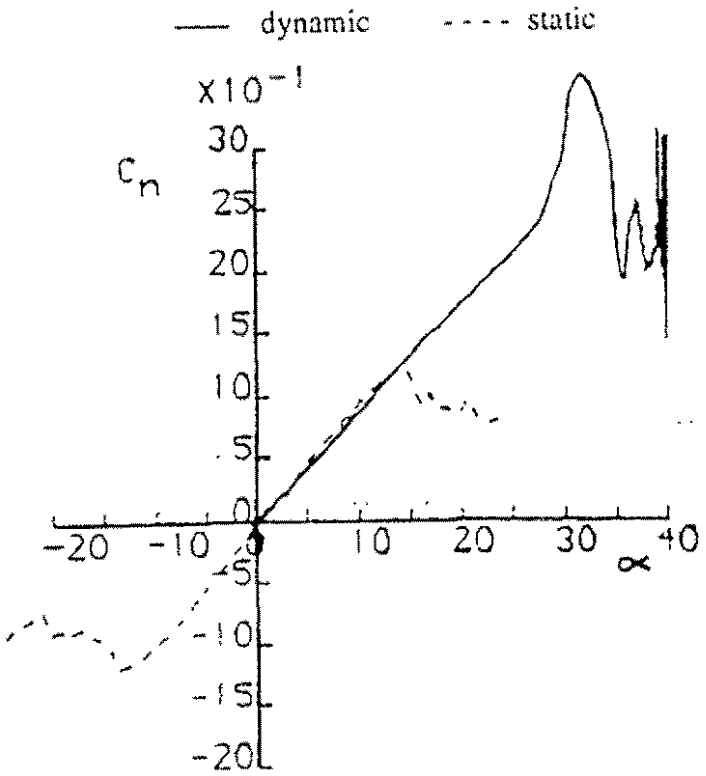

Ramp arc: -1° ~ 40°, R.P.R. = 0.0274, Re = 1.475×10 6

Fig.8 2-D Cn against α (NACA0015, Ramp Up)

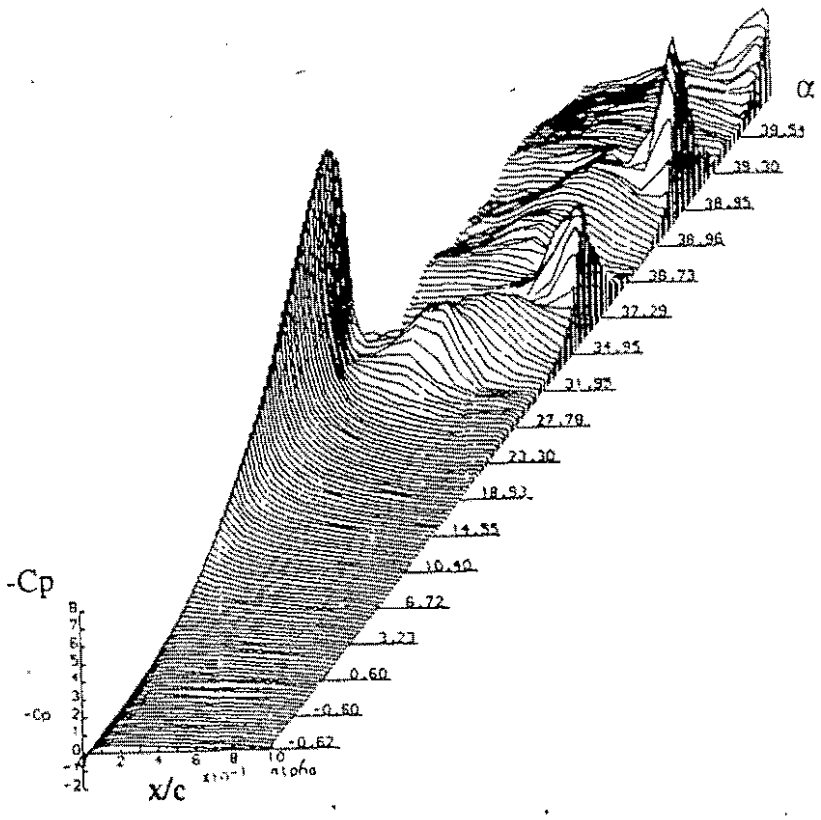

Ramp arc: -1° ~ 40°, R.P.R. = 0.0274, Re = 1.475×10 6

Fig.9 2-D Chordwise Cp against α (NACA0015, Ramp up)